Lymphatic regulator PROX1 determines Schlemm's canal integrity and identity

Dae-Young Park,[1] Junyeop Lee,[1] Intae Park,[1] Dongwon Choi,[2] Sunju Lee,[2] Sukhyun Song,[1] Yoonha Hwang,[3] Ki Yong Hong,[1] Yoshikazu Nakaoka,[4] Taija Makinen,[5] Pilhan Kim,[3] Kari Alitalo,[6] Young-Kwon Hong,[2] and Gou Young Koh[1]

[1]National Research Laboratory of Vascular Biology and Stem Cells, Graduate School of Medical Science and Engineering, Korea Advanced Institute of Science and Technology, Daejeon, Republic of Korea. [2]Department of Surgery, Department of Biochemistry and Molecular Biology, Norris Comprehensive Cancer Center, Keck School of Medicine, University of Southern California, Los Angeles, California, USA. [3]Graduate School of Nanoscience and Technology, Korea Advanced Institute of Science and Technology, Daejeon, Republic of Korea. [4]Department of Cardiovascular Medicine, Osaka University Graduate School of Medicine, Suita, Osaka, Japan. [5]Department of Immunology, Genetics and Pathology, Uppsala University, Uppsala, Sweden. [6]Molecular/Cancer Biology Laboratory, Biomedicum Helsinki, Department of Pathology, Haartman Institute and Helsinki University Central Hospital, University of Helsinki, Helsinki, Finland.

Schlemm's canal (SC) is a specialized vascular structure in the eye that functions to drain aqueous humor from the intraocular chamber into systemic circulation. Dysfunction of SC has been proposed to underlie increased aqueous humor outflow (AHO) resistance, which leads to elevated ocular pressure, a factor for glaucoma development in humans. Here, using lymphatic and blood vasculature reporter mice, we determined that SC, which originates from blood vessels during the postnatal period, acquires lymphatic identity through upregulation of prospero homeobox protein 1 (PROX1), the master regulator of lymphatic development. SC expressed lymphatic valve markers FOXC2 and integrin α_9 and exhibited continuous vascular endothelial–cadherin (VE-cadherin) junctions and basement membrane, similar to collecting lymphatics. SC notably lacked luminal valves and expression of the lymphatic endothelial cell markers podoplanin and lymphatic vessel endothelial hyaluronan receptor 1 (LYVE-1). Using an ocular puncture model, we determined that reduced AHO altered the fate of SC both during development and under pathologic conditions; however, alteration of VEGF-C/VEGFR3 signaling did not modulate SC integrity and identity. Intriguingly, PROX1 expression levels linearly correlated with SC functionality. For example, PROX1 expression was reduced or undetectable under pathogenic conditions and in deteriorated SCs. Collectively, our data indicate that PROX1 is an accurate and reliable biosensor of SC integrity and identity.

Introduction

Schlemm's canal (SC) is an endothelium-lined vascular channel that encircles the margin of the cornea and drains aqueous humor, which is produced in the ciliary body and supplies the cornea and lens with nutrients through collector channels into the circulation (1, 2). SC is a conventional aqueous humor outflow (AHO) pathway accounting for the majority of AHO and is responsible for appropriate resistance against it to maintain a balance between the secretion and drainage of aqueous humor, thereby controlling intraocular pressure (IOP) (3, 4). Uveoscleral tract, which includes the extracellular spaces within the iris, the ciliary muscle (CM), and sclera, is an unconventional AHO pathway and covers the egression of remaining aqueous humor (~20% in human, ~80% in mice) (5, 6). In physiologic conditions, conventional AHO is largely proportional to pressure, although unconventional AHO is relatively pressure independent (5). On the other hand, when the resistance of SC increases with age and disease reduces conventional AHO, IOP is elevated, thereby sometimes leading to irreversible ocular nerve damage and glaucoma (7).

▶ Related Commentary: p. 3701

Conflict of interest: The authors have declared that no conflict of interest exists.
Submitted: January 27, 2014; **Accepted:** May 30, 2014.
Reference information: *J Clin Invest*. 2014;124(9):3960–3974. doi:10.1172/JCI75392.

Lymphatic vessels (LVs) are lined by a single layer of lymphatic endothelial cells (LECs) and are responsible for draining tissue fluid into the circulation (8, 9). LECs are differentiated from blood endothelial cells (BECs) during early development, and the homeodomain transcription factor prospero homeobox protein 1 (Prox1) controls the BEC-to-LEC differentiation process. Notably, endothelial cell (EC) fate is found to be astonishingly plastic; ectopic expression of Prox1 in BECs induces lymphatic reprograming, while Prox1 deletion in LECs results in regaining of BEC fate in both embryonic and postnatal settings, labeling Prox1 as the master regulator for lymphatic cell-fate specification (8–12).

SC displays some important features found in LVs. Although originating from and directly connected to the blood vascular system, normal SC is devoid of blood-borne cells, such as red blood cells (13). SC controls the ocular tissue fluid homeostasis and tissue pressure by functioning as a major draining channel. Furthermore, the junction between SC ECs and trabecular meshwork (TM) is composed of a specialized tethering structure, which is responsible for providing an appropriate pressure gradient across the inner wall of an SC to maintain the integrities of SC ECs, thereby providing a tissue pressure-sensing/responding mechanism, such as anchoring filaments for LVs (14–16).

Despite SC's critical functions, its organogenesis and cell-fate–specification mechanism remain unclear. Here, we report that SC ECs, initially BECs, are postnatally respecified to acquire lymphatic

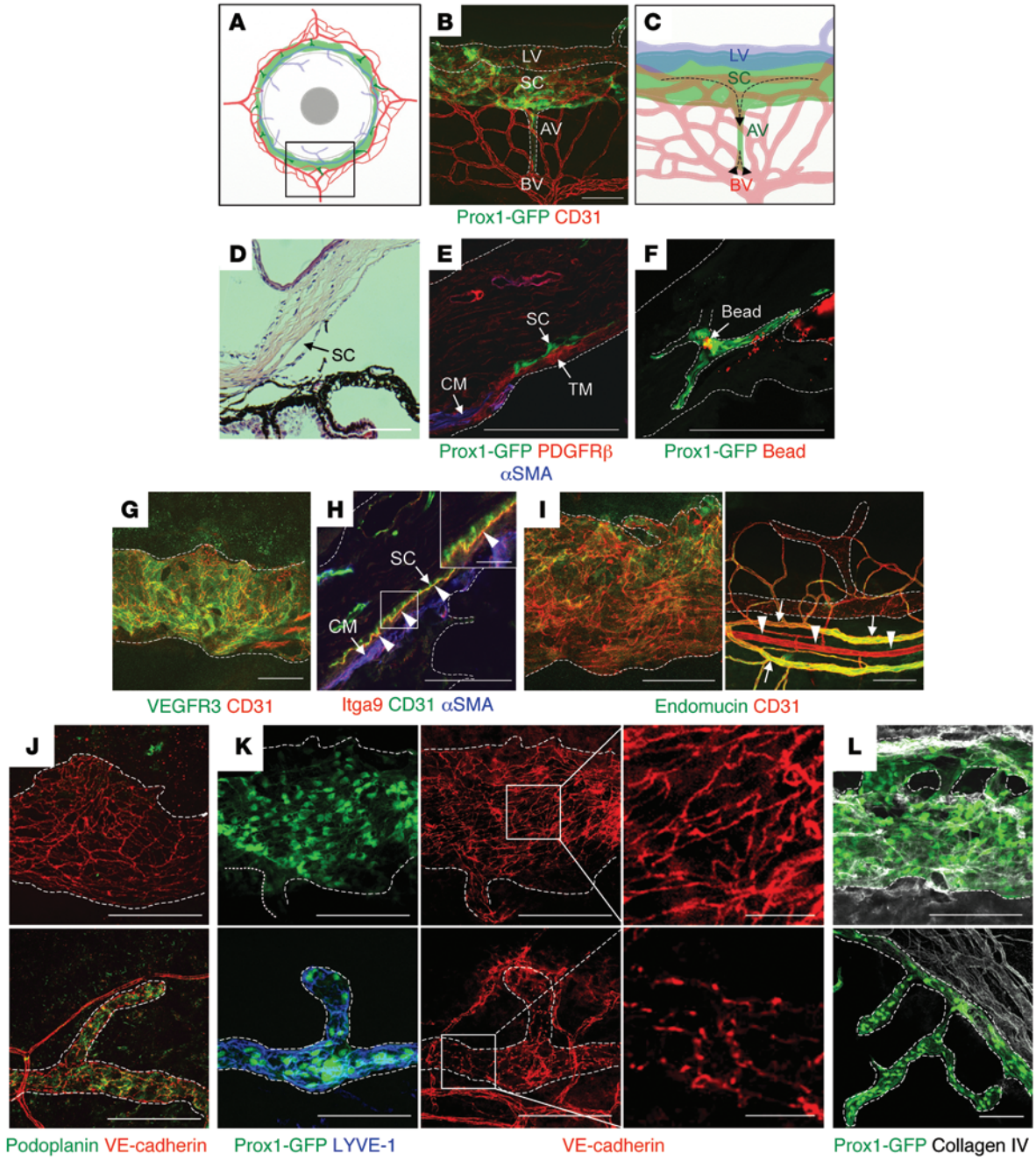

Figure 1. SC drains out aqueous humor into BVs and exhibits lymphatic markers but does not perfectly match the features of terminally differentiated LVs. (**A**) Schematic diagram of cornea showing SC (light green), AV (dark green), limbal LVs (light blue), and BVs (red). The square portion, immunostained and highly magnified, is shown in **B**. (**B** and **C**) Image and schematic diagram showing Prox1-GFP$^+$ SC, AV, and CD31$^+$ BV networks. Dashed lines demarcate limbal LV and AV, while dashed arrows indicate the AHO from SC into BVs. (**D**) H&E staining of corneal limbus in section. Arrow indicates SC. (**E**) Cross-sectioned image showing Prox1-GFP$^+$ SC, PDGFR-β$^+$ TM, and α-SMA$^+$ CM in corneal limbus. (**F**) Perfused red fluorescent microbeads (diameter, 1 μm) in Prox1-GFP$^+$ SC. Prox1-GFP mice were given 0.5 μl of the microbeads by intraocular injection; sample was harvested after 1 hour. (**G**) Image showing VEGFR3 expression in CD31$^+$ SC. (**H**) Cross-sectioned image showing Itga9 (arrowhead), CD31$^+$ SC, and α-SMA$^+$ CM in corneal limbus. Magnification of the square portion is shown in the top right corner. (**I**) Comparison of expression and distribution of endomucin between SC (left panel) and limbal LVs (right panel). Arrows indicate limbal veins, while arrowheads indicate limbal artery. (**J**–**L**) Comparisons of expressions and distributions of podoplanin, VE-cadherin, Prox1-GFP, LYVE-1, and collagen IV$^+$ basement membrane between SC (upper panels) and limbal LVs (lower panels). Dashed lines demarcate SC or limbal LVs (**I**–**L**).The square portions are magnified on the right. Scale bars: 100 μm; 20 μm (enlarged squares).

phenotypes by the upregulation of Prox1. We uncovered that AHO, but not VEGF-C/VEGFR3 signaling, is essential for the development and maintenance of SC integrity. Moreover, our pathology mimicking models with disrupted AHO manifested impairments in SC development as well as losses of its lymphatic characteristics. Above all, we detected synchronous fluctuations of Prox1 expression in SC with the changes of SC integrity and lymphatic characteristics, indicating Prox1 as a biosensor of SC integrity and identity.

Results

SC expresses the lymphatic-specific transcriptional factor Prox1. We first examined whether SC is detectable with lymphatic and blood vascular markers in the whole-mounted and cross-sectioned corneas of Prox1-GFP reporter mice (17). We confirmed that Prox1 was highly expressed in the CD31$^+$ SC and limbal LVs and moderately expressed in aqueous veins (AVs), which act as collecting channels between SC and episcleral blood vessels (BVs) (Figure 1, A–D, and Supplemental Video 1; supplemental material available online with this article; doi:10.1172/JCI75392DS1). The Prox1$^+$ SC was readily distinguishable from the PDGFRβ$^+$ TM and α-SMA$^+$ CM (Figure 1E). A bead passage assay revealed that the AHO could be traced within the Prox1$^+$ SC (Figure 1F). The SC also expressed VEGFR3 and endomucin, a venous EC marker (18), but lacked the expression of differentiated LEC markers, podoplanin and lymphatic vessel endothelial hyaluronan receptor 1 (LYVE-1) (19–21), whereas limbal LVs highly expressed podoplanin and LYVE-1 (Figure 1, G–K). In addition, SC showed segmental heterogeneities: the portion of SC adjacent to the bifurcation of long posterior ciliary arteries (LPCAs) displayed lower expressions of Prox1 and VEGFR3 and weaker drainage capacity (49%, 42%, and 84%, respectively), but stronger expression of vWF (3.6-fold), and was lacking α-SMA$^+$ CM compared with the SC located in other regions (Supplemental Figure 1, A–D). Importantly, SC displayed 2 structural features of collecting lymphatics: zipper-like continuous vascular endothelial–cadherin (VE-cadherin) junctions (22) and collagen IV$^+$ basement membrane (ref. 23 and Figure 1, K and L). In contrast, the limbal LVs (capillaries) demonstrated button-like discontinuous VE-cadherin junctions without basement membrane investment (Figure 1, K and L). Interestingly, however, the ECs of SC expressed the lymphatic valve markers Foxc2 (Supplemental Figure 2, A and B, and ref. 24) and integrin α_9 (Itga9) (Figure 1H and ref. 25), even though SC did not have luminal valves in its lumen according to our observations of the blood regurgitation from BVs to SC following an ocular puncture (Supplemental Figure 3, A and B). Thus, SC is a unique vascular structure composed of collecting LV-like assembly of ECs, which can be detected with Prox1.

SC acquires lymphatic signatures during postnatal development. To elucidate how SC is formed, we examined the morphological changes of primitive SCs and their expression patterns of angiogenic (or lymphangiogenic) growth factor receptors during postnatal development. Initial endothelial buds of SC derived from choroidal veins (CVs) were detected at P1 (Figure 2A). The CVs expressed VEGFR2, VEGFR3, and Tie2, and these expressions were retained in the ECs of primitive SC at P1 (Figure 2, A and B). At P4, the ECs of elongated primitive SC became fused and separated from the CVs with the start of Prox1 expression (Figure 2A). However, Sox18, an upstream inducer of Prox1 in the cardinal vein (Supplemental Figure 4A and ref. 26), was not detected in the ECs of SC at P1 and P4 (Supplemental Figure 4B). To trace the development of SC, we performed a serial intravital imaging of the SC in Prox1-GFP mice. Active sprouting from preexisting SC was still detected at P7–P8 (Supplemental Figure 5), and the SC area grew gradually until 2 months of age (Figure 2, A and B). Moreover, while Prox1 expression rapidly and concomitantly increased with VEGFR3 in SC from P4 to adulthood, the expressions of BV markers VEGFR2 and Tie2 gradually decreased (Figure 2, A and B). Additionally, we evaluated the temporal change of Foxc2 expression in SC compared with that in limbal LVs. In the limbal LVs, Foxc2 was expressed in the developing LECs at P7 and in the lymphatic valves after P14 (Supplemental Figure 2A). Although the initial endothelial bud of SC lacked Foxc2 expression, Foxc2 expression emerged around P7 (Supplemental Figure 2B). Intriguingly, some Prox1$^+$ SC ECs were devoid of Foxc2 expression until adulthood, but for ECs that expressed Foxc2, it was mainly colocated with the expression of Prox1 (Supplemental Figure 2B). Collectively, primitive SC acquires lymphatic phenotype through lymphatic reprogramming, which we speculate to be activated by a certain stimulus during postnatal development.

AHO regulates morphogenesis and lymphatic fate of SC during development. We hypothesized that the initiation (and increase) of AHO through SC might be a major factor for its growth and Prox1 expression during development. To address the effect of AHO on SC development, we utilized an ocular puncture model (Figure 2C). To reduce the AHO through SC, eyes were punctured daily from P5, causing an artificial leakage of aqueous humor through the puncture (Figure 2C). After the puncture of the eye, IOP dropped by 34% compared with the contralateral sham-operated eye (hereafter called "control eye") (Figure 2D). As a result, the SC area, the protein and mRNA levels of PROX1, and the VEGFGR3 protein level in SC at P7 decreased by 61%, 69%, 74%, and 68%, respectively, in the punctured eye compared with the control eye (Figure 2, E–G). In addition, the reduction of AHO by a single puncture decreased the PH3$^+$ proliferating ECs by 57%, while it increased the caspase-3$^+$ apoptotic ECs by 5.2-fold at P6 in the growing SC of the punctured eye compared with that of control eye (Figure 3, A–C). Furthermore, a long-term reduction of AHO and subsequently decreased IOP induced by punctures from P4 to P14 also reduced the SC area (58%) and Prox1 expression (70%) (Supplemental Figure 6, A–D). In addition, we applied Cosopt from P5–P7, a drug that is conventionally used for lowering IOP in glaucoma patients by inhibiting aqueous humor production in the ciliary body (27) (a combined agent of β-adrenergic receptor inhibitor and carbonic anhydrase inhibitor), as an alternative method to decrease IOP (16% at P7) to confirm our findings with the ocular puncture model. Similar to the findings of the ocular puncture model, the SC area and protein and mRNA levels of PROX1 were reduced by 21%, 54%, and 47%, respectively, at P7 compared with the control eye (Figure 3, F–I). Conversely, to increase AHO during SC development, eyes were injected with donor aqueous humor once at P6. We found that the IOP was significantly elevated by 1 hour after the injection compared with the contralateral sham-operated eye (control eye), but returned to baseline IOP after 24 hours (Figure 3J). Consequently, the SC area was increased by 11% at P7 in the injected eye compared with the control eye (Figure 3, K and L). Also, the SC in the injected eye tended to have increased PROX1 and VEGFR3 protein levels, but without any significance (Figure 3, K and M). These findings support the hypothesis that incremental AHO positively regulates the development of SC.

Analysis of the molecular basis of AHO-mediated lymphatic reprograming in SC. We therefore investigated the molecular mechanisms underlying the flow-mediated lymphatic reprograming in SC ECs. Among a number of genes regulated by flow (Supplemental

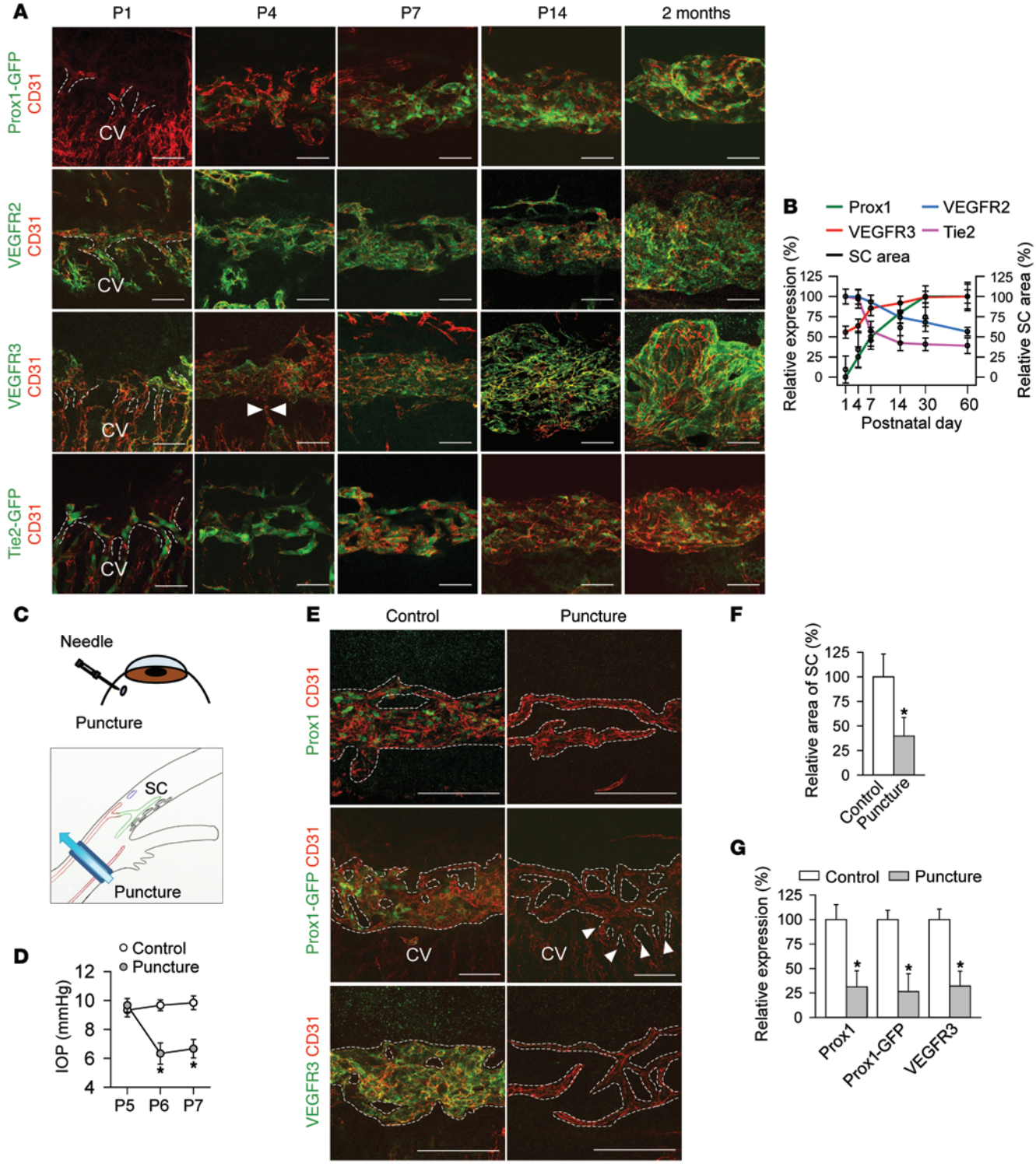

Figure 2. Acquisition of lymphatic characteristics in SC dependent on AHO during postnatal development. Unless otherwise noted, for the bar graphs, the quantification of the control group was normalized to 100%, from which the quantifications of other groups were calculated. (**A** and **B**) Temporal changes and quantifications of SC area and expression of Prox1, VEGFR2, VEGFR3, and Tie2 in SC during postnatal development. Dashed lines indicate the buds of SC derived from the CVs. Arrowheads demarcate the remnant communication between SC and CVs. Mean ± SD are shown (n = 4). Scale bars: 50 μm. For the quantifications, the group with the highest value was normalized to 100%, from which the relative values of other groups are shown. (**C**) Schematic diagram showing generation of the ocular puncture. Upper panel: a puncture on the sclera through 31-gauge syringe needle; lower panel: reduction of AHO achieved by leakage through the puncture. (**D**–**G**) Images and comparisons of the SC between the punctured eyes (puncture) and the sham-operated control eyes. Eyes were punctured from P5 to P6, and the corneas were harvested at P7. (**D**) Comparison of IOP. Each group, n = 4–5. (**E**) Images showing Prox1$^+$, Prox1-GFP$^+$, or VEGFR3$^+$ cells in CD31$^+$ SC. Arrowheads indicate the remnant communication between SC and CVs. Scale bars: 100 μm. (**F** and **G**) Comparisons of relative area and expressions of Prox1, Prox1-GFP, and VEGFR3 in SC. Each group, n = 4–5. *P < 0.05 versus control.

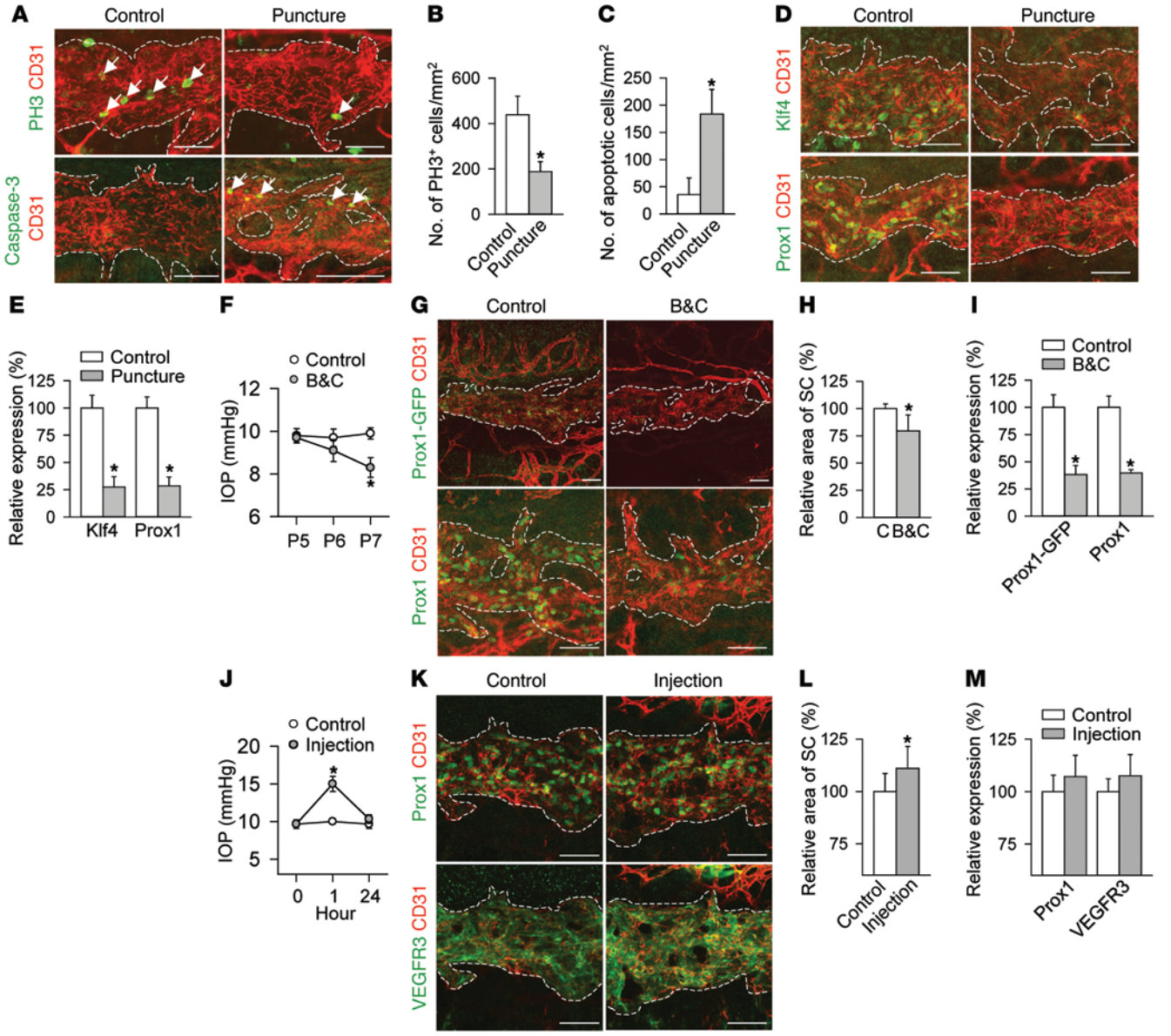

Figure 3. AHO determines the expansion of SC ECs during postnatal development. Unless otherwise noted, the relative SC area and expression in control was normalized to 100%, from which the relative expressions of other groups were calculated. $n = 4$, each group. (**A**–**E**) Images and comparisons of the SC between punctured eyes and control eyes. Eyes were punctured at P6 and harvested at P7. (**A** and **D**) Images showing the expression of PH3, caspase-3, Klf4, and Prox1 in SC. (**B**, **C**, and **E**) Comparison of numbers of PH3$^+$ cells and caspase-3$^+$ cells, and relative expressions of Klf4 and Prox1 in SC. (**F**–**I**) Eyes of WT and Prox1-GFP mice were treated with control buffer (control) or Cosopt (B&C) daily from P5 to P7, and corneas were harvested at P7. (**F**) Comparison of IOP. (**G**) Images showing expression of Prox1-GFP and Prox1 in SC. (**H** and **I**) Comparison of relative SC area and expression of Prox1-GFP and Prox1. (**J**–**M**) Images and comparisons of the SC between injected eyes (injection) and sham-operated eyes (control). Eyes were injected with donor aqueous humor at P6 and harvested at P7. (**J**) Comparison of IOP. (**K**) Images showing Prox1 and VEGFR3 expression in SC. (**L** and **M**) Comparison of relative SC area and expression of Prox1 and VEGFR3 in SC. Scale bars: 50 μm. *$P < 0.05$ versus control.

Table 1), *Klf4*, which was previously identified as a key shear stress–responsive transcription factor (28), attracted our attention as it was also highly upregulated in our RNA-Seq analyses. Accordingly, we confirmed the Klf4 expression in the nuclei of corneal epithelium (29) and ECs of SC, limbal BVs, and limbal LVs at P5, and, importantly, Klf4 expression was found to precede Prox1 expression in SC (Supplemental Figure 6E), indicating a possible existence of flow before the completion of lymphatic differentiation of SC. This relationship between Klf4 and Prox1 was confirmed with an in vivo ocular puncture model that showed that the expressions of Klf4 and Prox1 concomitantly decreased by 73% and 72%, respectively, in the punctured eye compared with the control eye (Figure 3, D and E). Moreover, the reduction of AHO caused by punctures in the earlier postnatal period (P3 to P5) retarded SC development, resulting in a 53% reduction in the SC area and 64% and 62% decreased expressions of Prox1 and Klf4, respectively, in the punctured eye compared with the control eye (Supplemental Figure 6, F–H).

We questioned whether the shear stress–responsive transcription factor Klf4 may play a role in the AHO-mediated Prox1 upregulation. We first confirmed that laminar flow (~2 dyne/cm^2)

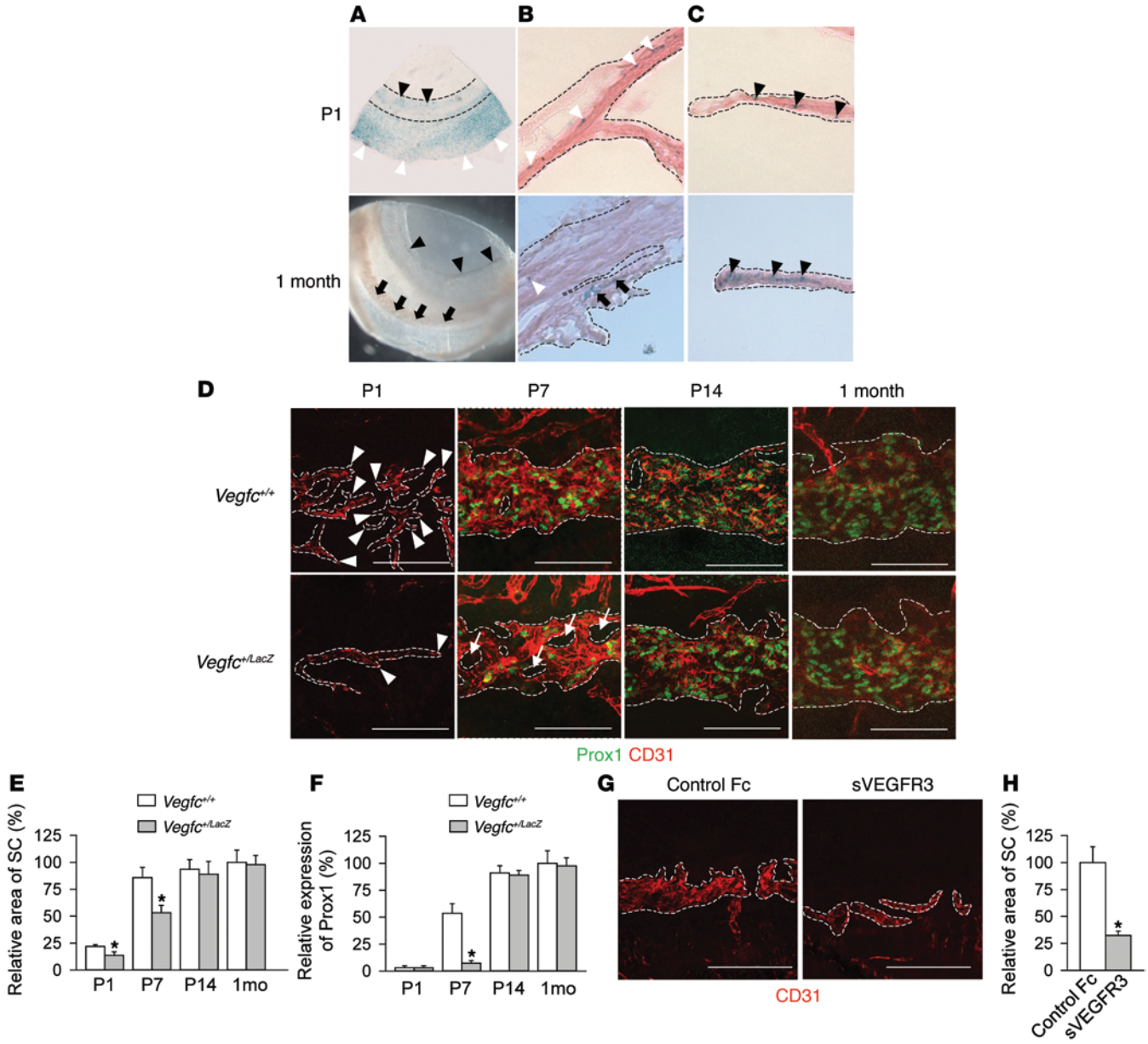

Figure 4. VEGF-C/VEGFR3 system plays a crucial role in the early development of SC. (**A**–**C**) β-Gal staining of corneas in VEGF-C–β-gal knockin reporter mice (*Vegfc*$^{+/LacZ}$) at P1 and 1 month. Robust VEGF-C expression in superficial layer of cornea (white arrowhead) and iris (black arrowhead) at P1 is shown, while rarer VEGF-C expression in TM (black arrow) and iris (black arrowhead) at 1 month is shown. (**D**) Prox1 and CD31 staining of SC ECs in *Vegfc*$^{+/LacZ}$ and *Vegfc*$^{+/+}$ mice during postnatal development. Arrowheads indicate buddings of SC ECs. Arrows indicate holes in SC, which denote defects of tubular fusion. (**E** and **F**) Comparisons of relative area and Prox1 expression of SC. The area and Prox1 expression of *Vegfc*$^{+/+}$ at 1 month was set as 100%, respectively. $n = 4$, each group. *$P < 0.05$ versus *Vegfc*$^{+/+}$. (**G** and **H**) Mice were i.p. given sVEGFR3 (25 mg/kg) daily from P1 to P6 and designated as control Fc and sVEGFR3; corneas were harvested at P7. (**G**) Image showing CD31^{+} SC ECs. (**H**) Comparison of relative SC area. The quantification of control Fc group was normalized to 100%, from which the quantifications of other groups were calculated. $n = 4$, each group. *$P < 0.05$ versus control Fc. Scale bars: 100 μm.

efficiently upregulated Klf4 expression in cultured postnatal human dermal BECs and LECs within 12 hours (Supplemental Figure 7A). However, this specific in vitro experimental condition neither activated Prox1 expression in postnatal BECs, nor altered the expression level of Prox1 in postnatal LECs (Supplemental Figure 7A). Consequently, because 2 previous genome-wide ChIP studies (30, 31) have suggested a possible binding of *Klf4* to the *Prox1* gene, we next questioned whether KLF4 protein could bind to putative *Prox1* enhancer regions. Indeed, our ChIP-PCR analyses revealed that 12-hour–long laminar flow could physically associate KLF4 protein with a putative enhancer area (chr1:212,229,489–212,229,614) in the first intron of the *Prox1* gene of BECs (Supplemental Figure 7B), indicating that KLF4 protein is recruited to the Prox1 regulatory region in BECs under the shear stress condition. Despite this protein/DNA interaction, however, adenoviral overexpression of Klf4 did not turn on the expression of Prox1 in BECs (Supplemental Figure 7C). Moreover, we cloned the Klf4-binding area of the *Prox1* gene in

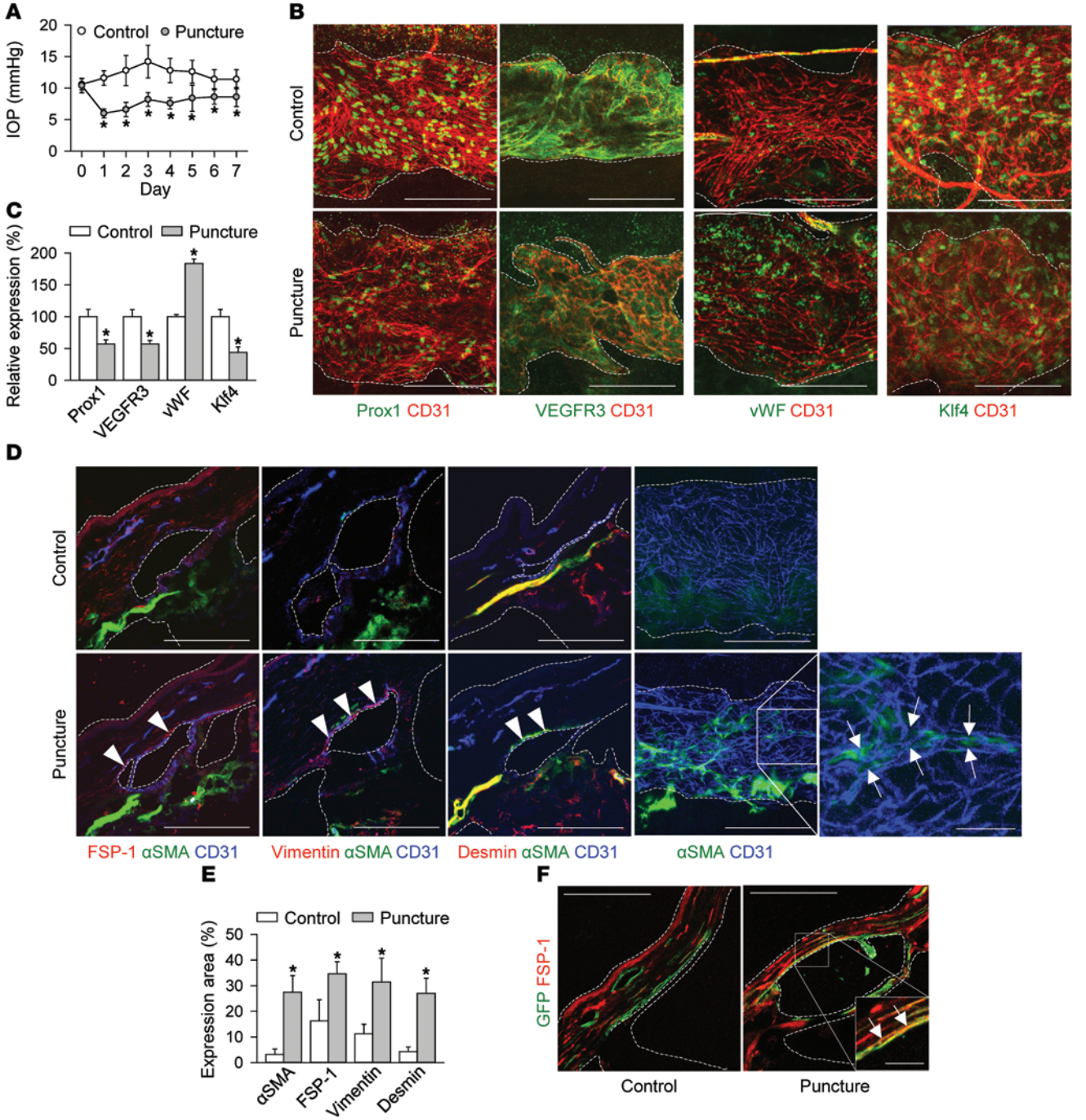

Figure 5. Reduced AHO induces loss of lymphatic feature in SC ECs, leading to EndMT. (**A**–**E**) Images and comparisons of SC between punctured eyes and sham-operated control eyes. Eyes were punctured daily for 7 days, and corneas were harvested at day 7. (**A**) Comparison of IOP. n = 4–5, each group. (**B** and **C**) Images and comparisons of expressions of Prox1, VEGFR3, vWF, and Klf4 in the CD31$^+$ ECs of SC. n = 4–5, each group. The quantification of control group was normalized to 100%, from which the quantifications of other groups were calculated. (**D** and **E**) Images and comparisons of mesenchymal markers α-SMA, FSP-1, vimentin, and desmin in CD31$^+$ SC ECs. Solid-line square is magnified on the right, which reveals α-SMA expression in the CD31$^+$ EC of SC (white arrows). Arrowheads indicate expression of FSP-1, vimentin, and desmin in CD31$^+$ SC ECs, respectively. n = 4–5, each group. (**F**) Lineage-tracing study in which *Prox1-Cre^{ERT2} R26mTmG* mice were treated with tamoxifen 3 times from 8 weeks. Then eyes were punctured daily for 7 days, and corneas were harvested at day 7. Solid-line square is magnified in the bottom right corner. Arrows indicate coexpression of FSP-1 in GFP$^+$ SC ECs. *P < 0.05 versus control. Scale bars: 100 μm; 20 μm (enlarged squares).

the pGL3-promoter vector to assess the capability of Klf4 to activate the luciferase reporter through its binding region. However, Klf4 could not activate the expression of the luciferase reporter (Supplemental Figure 7D). These data indicate that although Klf4 acquires a binding affinity to the Prox1 regulatory region in BECs in response to shear stress, the employed experimental condition was not sufficient for Klf4 to switch on the otherwise silenced Prox1 expression in BECs.

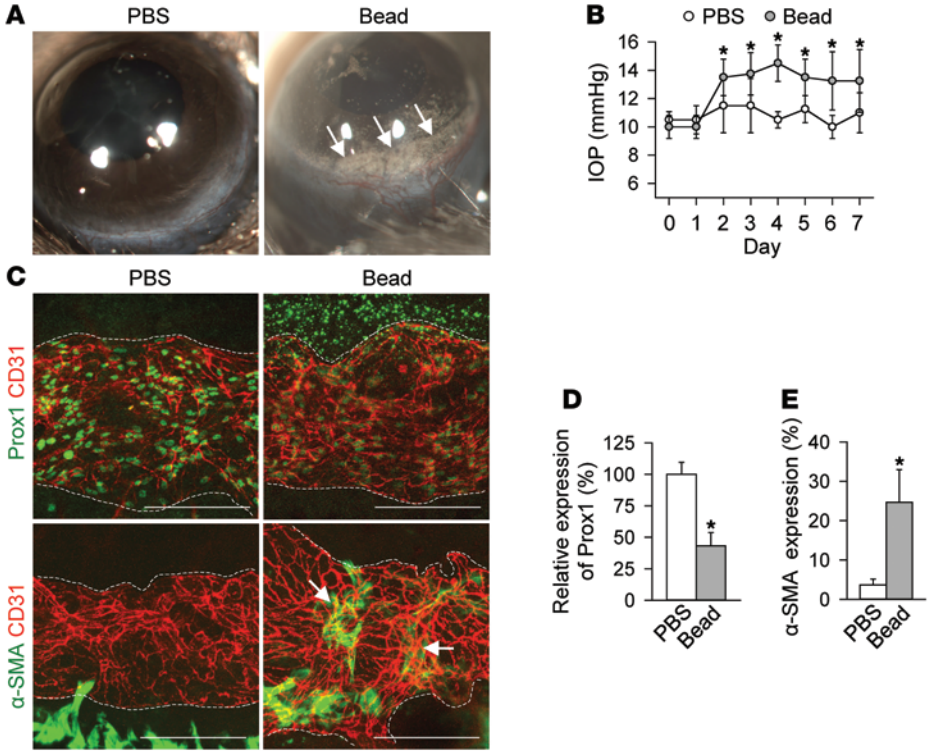

Figure 6. Analysis of lymphatic identity in SC with defective AHO within bead-induced glaucoma model. (**A**–**E**) Eyes were injected with 2 μl of microbeads (bead diameter, 6 μm) or 2 μl of PBS, and corneas were harvested after 7 days. (**A**) Appearance of a bead-injected eye. Arrows indicate deposited beads adjacent to SC. (**B**) Comparison of IOP. $n = 4$, each group. (**C**) IHC of SC stained for Prox1 and α-SMA in CD31$^+$ SC. Scale bars: 100 μm. (**D** and **E**) Comparisons of relative Prox1 expression and of the coverage of α-SMA$^+$ cells by measuring α-SMA$^+$ area divided by CD31$^+$ SC area, expressed as a percentage. The relative expression of PBS was normalized to 100%, from which the relative expressions of other groups were calculated. $n = 4$, each group. *$P < 0.05$ versus PBS.

Next, we investigated the role of integrin β_1 during SC development because integrin β_1–mediated VEGFR3 phosphorylation in response to fluid acquisition has been known to trigger LV expansion (32). After confirming the presence of integrin β_1 in SC ECs, limbal BVs, and CM (Supplemental Figure 8A), mice were i.p. treated with anti–integrin β_1 functional blocking antibody (25 mg/kg) from P1 to P6 and harvested at P7. We confirmed the antiangiogenic effect (33) caused by the suppressed growth of retinal BVs as shown by decreased radial length of BVs and number of filopodia (10% and 25%, respectively) compared with control mice (Supplemental Figure 8, B–D). Meanwhile, the analysis showed no differences in the SC area or expression of Prox1 and VEGFR3 (Supplemental Figure 8, E–G), indicating that the blockade of integrin β_1 was not sufficient to affect the growth and lymphatic identity of SC.

VEGF-C/VEGFR3 system plays a substantial role in the early development of SC. To explore the significance of VEGF-C/VEGFR3 signaling in SC development, we checked the expression pattern of VEGF-C by using VEGF-C–β-gal knockin reporter mice (*Vegfc*$^{+/LacZ}$) (34). We observed that VEGF-C was highly expressed in the superficial layer of the cornea and iris at P1, whereas its expression was detected in the iris and the junctional tissue between SC and TM during adulthood (Figure 4, A–C). In addition, compared with control mice (*Vegfc*$^{+/+}$), *Vegfc*$^{+/LacZ}$ mice displayed delayed buddings of SC ECs from the CVs, retarded tubular fusion, smaller SC area (38% at P1 and 38% at P7), reduced Prox1 expression (87% at P7), and markedly diminished limbal LVs (99%) during postnatal development (Figure 4, D–F, and Supplemental Figure 9, A and B). In line with these results, we confirmed that daily i.p. injection of soluble VEGFR3-Fc (sVEGFR3-Fc) (25 mg/kg) from P1 to P6 markedly reduced the area of SC and limbal LVs (68% and 69%, respectively) at P7 (Figure 4, G and H, and Supplemental Figure 9, C and D). Regardless of the severe outcomes of VEGF-C/VEGFR3 signaling disruption during SC development, the SC of *Vegfc*$^{+/LacZ}$ had well-organized morphology, normalized SC area, and recovered Prox1 expression by P14 compared with *Vegfc*$^{+/+}$ (Figure 4, D–F), whereas the limbal LVs were still affected (Supplemental Figure 9, E and F).

Reduced AHO induces a loss of lymphatic characteristics in SC, leading to EndMT. As AHO often decreases due to aging and pathological insults (2), we next investigated the requirement of AHO in the maintenance of the lymphatic identity of SC in adults using the murine eye puncture model. Puncture was made in the sclera of adult mice daily for 7 days to decrease their IOP (Figure 5A). Compared with the SC of the control eye, the SC of the punctured eye exhibited reduced expressions of Prox1 (43%), VEGFR3 (43%), and Klf4 (56%), whereas they displayed increased expressions of vWF (1.8-fold), α-SMA (8.7-fold), fibroblast-specific protein 1 (FSP-1) (2.1-fold), vimentin (2.8-fold), and desmin (6.3-fold) (Figure 5, B–E). We also noted that α-SMA expression was colocalized with the CD31$^+$ area of SC ECs in the punctured eye (Figure 5D).

To trace the fate of ECs in SC, we performed a lineage-tracing study with *Prox1-Cre*^{ERT2} *Rosa26mTmG* mice, in which Prox1-expressing cells retained permanent membrane GFP expression after tamoxifen injection. Following the daily puncture of eyes over 7 days, the GFP$^+$ SC ECs partly exhibited FSP-1 expression, whereas no FSP-1 expression was observed in that of control eye (Figure 5F). These findings indicate that the ECs of SC undergo endothelial-mesenchymal transition (EndMT) (35–37) when the AHO through SC is reduced. To support our data, which suggest that AHO is critical for the maintenance of lymphatic characteristics in SC, we created an experimental glaucoma model using beads (6 μm in diameter) that blocks the AHO and elevates the IOP (38). One day after

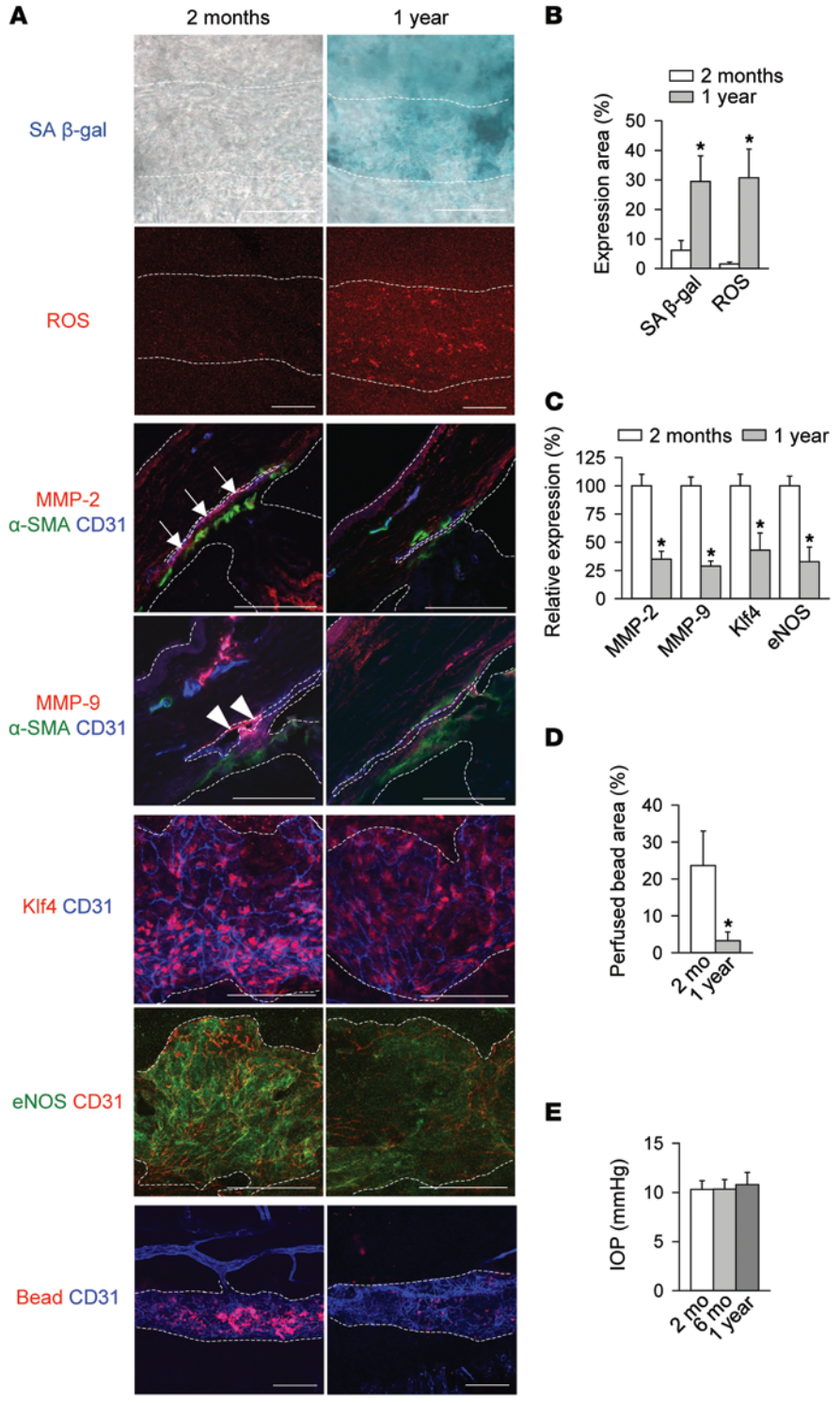

Figure 7. Aged SC exhibits features of senescent endothelium and reduced AHO. (**A**–**D**) Images and comparisons of expressions in SA β-gal, ROS, MMP-2, MMP-9, Klf4, eNOS, and perfused microbead (bead) in SC of 2-month-old and 1-year-old mice. Arrows and arrowheads indicate expressions of MMP-2 and MMP-9, respectively, in CD31⁺ SC. The relative expression of SC at 2 months was normalized to 100%, from which the relative expressions of other groups were calculated. $n = 5$, each group. *$P < 0.05$ versus 2 months. (**E**) Comparisons of IOP at 2, 6, and 12 months. $n = 5$, each group. Scale bars: 100 μm.

the intraocular injection of the beads, an accumulation of these beads was notable around the margin of the cornea (Figure 6A). Compared with the PBS-injected eyes, the IOP of the bead-injected eyes remained elevated (Figure 6B), and the Prox1 expression was reduced by 57%, while the α-SMA expression increased by 6.8-fold in their SC (Figure 6, C–E).

Aged SC displays the features of senescent endothelium and reduced lymphatic markers as well as increased mesenchymal markers. SCs are constantly exposed to external stress over a lifetime (39), which suggests that they may be undergoing the aging process faster than any other organs. In fact, in the SC of 1-year-old mice, the activities of senescence-associated β-gal (SA–β-gal) and ROS were markedly upregulated in the SC, by 4.8- and 20.3-fold, respectively, whereas the expressions of MMP-2 and MMP-9 in the junctional tissue between SC and TM were downregulated by 65% and 71%, respectively, and the AHO was reduced by 86% along with the 57% and 67% suppressed expressions of Klf4 and eNOS, respectively, compared with the SC of 2-month-old mice (Figure 7, A–D). Nevertheless, no significant differences in the IOP between the young and old mice were detected (Figure 7E), in agreement with previously reported knowledge (40). We assumed that this is because uveoscleral AHO has a greater role in mice, accounting for approximately 80% of the total AHO, thereby compensating for the dysfunctional drainage through SC, unlike in humans (6).

In terms of LEC markers, compared with the SC of 2-month-old mice, the SC of 1-year-old mice exhibited 59%, 65%, 55%, and 67% less expression of Prox1, Prox1-GFP, VEGFR3, and Itga9, respectively, while vWF expression was 2.1-fold higher (Figure 8, A and B). Consistent with this, we confirmed a 62% decreased *Prox1* mRNA level in the corneal limbus, as shown by RT-PCR (Figure 8C). These findings indicate that the lymphatic identity of the SC is suppressed in aged mice. Furthermore, the SC of 1-year-old mice exhibited an 11.0-fold increase in α-SMA expression compared with that of 2-month-old mice (Figure 8, A and D). Most of the α-SMA⁺ cells appeared to be star shaped and mimicked fibroblasts. Furthermore, the analyses in the SC of 1-year-old mice showed 3.0-fold and 13.6-fold increased expressions of

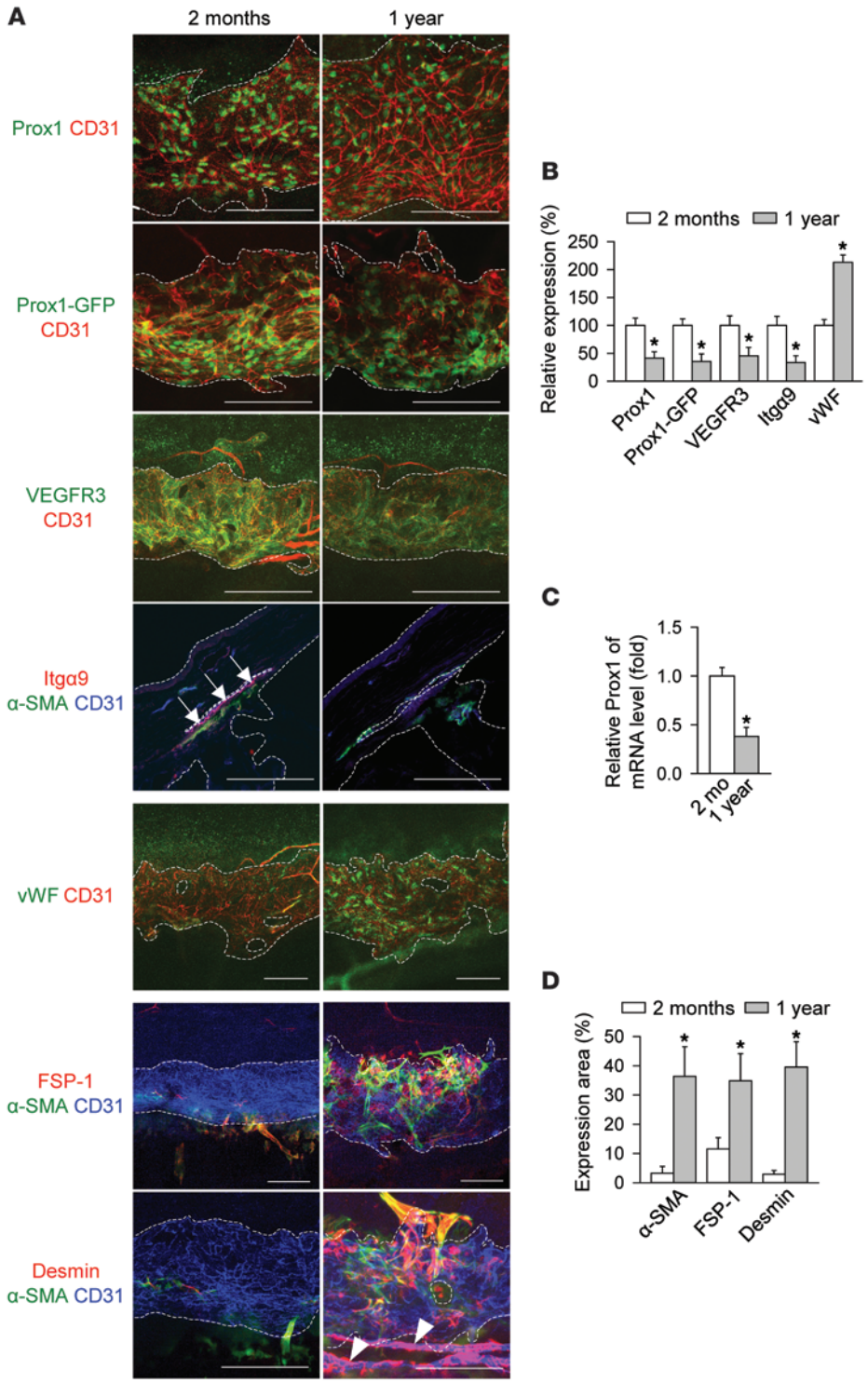

Figure 8. Aged SC displays reduced lymphatic markers and increased mesenchymal markers. (**A**, **B**, and **D**) Images and comparisons of expression in Prox1, Prox1-GFP, VEGFR3, Itga9, vWF, FSP-1, α-SMA, and desmin in CD31⁺ SC of 2-month-old and 1-year-old mice. Arrows indicate Itga9 expression in CD31⁺ SC. Arrowheads denote CD31⁺ limbal BVs with desmin coverage. The relative expression of SC at 2 months was normalized to 100%, from which the relative expressions of other groups were calculated. $n = 5$, each group. $^*P < 0.05$ versus 2 months. (**C**) Comparisons of *Prox1* mRNA expressions in corneal limbus. $n = 5$, each group. $^*P < 0.05$ versus 2 months. Scale bars: 100 μm.

FSP-1 and desmin, respectively, both of which were partially correlated with α-SMA expression (Figure 8, A and D). Collectively, senescent SC showed analogous phenotypes to SC in punctured eyes, which might be manifested by the long-term suppression of AHO (Figure 9).

Discussion

Heterogeneity and plasticity are the two most important features of ECs (41). ECs often respond to physiological stimuli and pathological insults by altering their cell fates. This astonishing cell-fate plasticity is believed to underlie the remarkable heterogeneity of ECs. ECs of SC in the eye have long been suspected as being distinct from BECs of the capillaries or postcapillary venules, mainly because SC drains and carries tissue fluids (aqueous humor), not blood, although directly connected to BVs. Here, we report that SC ECs originate from the CVs and undergo a partial lymphatic reprogramming during postnatal development, giving rise to a novel class of ECs that display both BEC and LEC phenotypes. SC ECs express a list of key lymphatic-signature genes, such as *Prox1*, *Vegfr3*, and *Itga9* (10), along with the venous marker endomucin (18), but, most notably, lack expressions of podoplanin and LYVE-1 (Figure 9). In fact, it is known that podoplanin, but not LYVE-1, is regulated by *Prox1* (41, 42). However, the nonexistent expressions of both genes in SC ECs, despite the presence of Prox1 expression, is quite unusual and striking, since podoplanin and LYVE-1 are predominantly expressed in capillary LECs (43, 44), raising a possibility that SC ECs may not be terminally differentiated from LECs and their lymphatic phenotype may be intermediate. This possibility is further supported by our findings that Prox1 expression levels in SC ECs, but not in the limbal LVs, are dynamically regulated by AHO and aging. Additional unusual features of SC compared with normal LVs are that it displays structural features of collecting lymphatics (zipper-like continuous VE-cadherin junctions, ref. 22; and

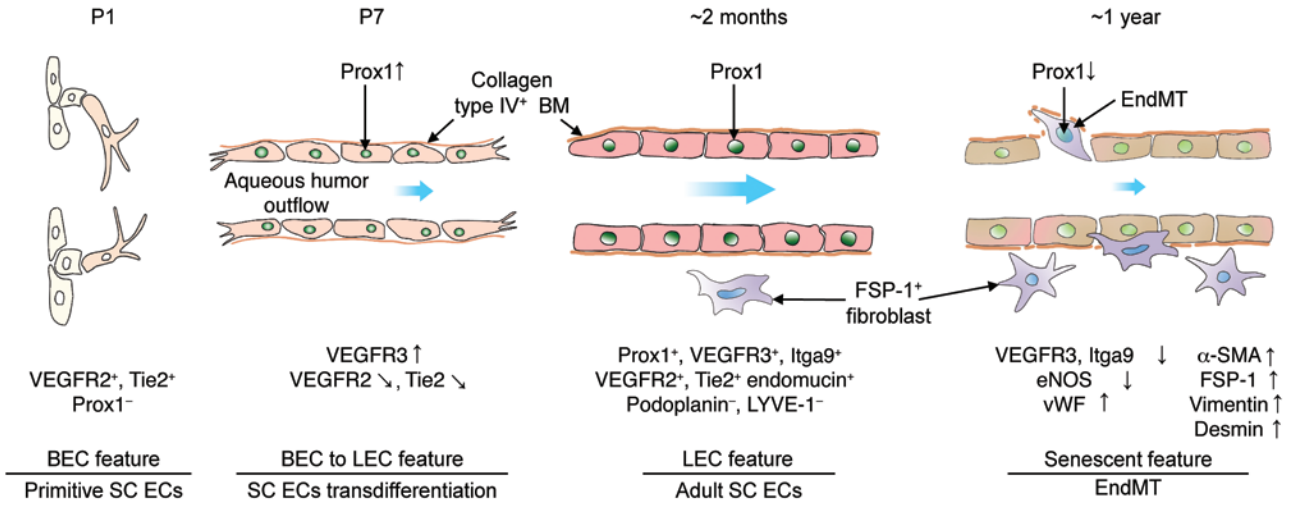

Figure 9. Schematic diagram depicting the dynamic changes of lymphatic identities of SC during development, adulthood, and senescence. SC ECs are postnatally transdifferentiated from BECs (VEGFR2⁺, Tie2⁺, and Prox1⁻) to acquire lymphatic phenotypes by the upregulation of Prox1 and increased AHO. With ageing, senescent SC ECs, which by then have reduced AHO, start to lose lymphatic markers (Prox1, VEGFR3, and Itga9), but gain blood vessel markers (vWF) as well as mesenchymal markers (α-SMA, FSP-1, vimentin, and desmin), leading to EndMT.

collagen IV⁺ basement membrane, ref. 23) without luminal valves, a hallmark of the collectors (25). All these data cohesively suggest that SC is a specialized vascular structure that displays some lymphatic phenotypes and carries out lymphatic function, but is distinct from normal LVs (Figure 9).

Interesting similarities can be found between embryonic lymphatic development and postnatal lymphatic differentiation of SC in terms of their formation. Both processes involve progenitor cell migration from the veins and subsequent acquisition of lymphatic phenotypes (45). Also, Prox1 appears to play a key role in both cell-reprograming events. The differentiated progenitor cells assemble to form new tubular structures, which later dissociate from the veins. Our current study found that AHO is essential for all stages of SC development as well as maintenance of its lymphatic phenotypes, which is also the case for lymphatic development (32). However, one major difference is that while Prox1 is upregulated in cardinal vein ECs before they migrate out during embryogenesis, Prox1 expression begins in the primitive SC structure, not in the CVs, at P4 and continues to increase until mice are 1 month old. In particular, Sox18 expression was absent in SC during early postnatal development, but present in the cardinal vein during embryonic lymphangiogenesis (26). It remains to be defined whether and how these differences affect the cell-fate specification as well as expression of lymphatic markers such as podoplanin and LYVE-1 (41).

Importantly, Prox1 expression in SC ECs was found to be highly sensitive to AHO; reduction in AHO induced by our surgical (ocular puncture model) or noninvasive (pharmacological) approach consistently downregulated Prox1. Although the strategy to increase AHO with incremental IOP over a long duration (>24 hours) was not successful, attributed to the small volume of the eyes of pups limiting the injection of adequate amount of aqueous humor, transiently elevated IOP tended to upregulate Prox1 and VEGFR3. Moreover, segmental heterogeneity in Prox1 expression was also found in the normal cornea; a weaker Prox1 expression was found in disorganized sections in SC with decreased AHO due to lack of CM (13), which were frequently found adjacent to the bifurcation portion of LPCAs. Furthermore, senescent SCs, which are similar to those of aged humans (46), showed a deficiency of lymphatic markers and increased density of mesenchymal cells, similar to the aftermath of artificially reduced AHO models. Previous studies reported that the inner wall of SC is the principal site of flow resistance against AHO (14). Furthermore, AHO resistance between SC and TM has been found to increase with age in humans (2). Indeed, senescent ECs in old mice involve disturbed AHO, coinciding with the dysfunction of MMP activities, which are responsible for ECM remodeling of the junction between SC and TM to maintain the appropriate AHO resistance (47). Consequently, the impairment of AHO through SC with aging leads to suppressed lymphatic identity and loss of EC integrity in SC. Overall, we propose that deficient AHO negatively affects the lymphatic fate of SC ECs.

Hemodynamic forces have been postulated to maintain the integrities of BVs (48). The importance of mechanotransduction in response to gain of fluid was highlighted in LEC proliferation via VEGFR3 activation (32). Previous studies comprehensively predicted the existence of a fluid-induced mechanistic factor in LECs (24, 49, 50). Furthermore, lymphatic vascular integrity can be compromised by a dose-dependent Prox1 depletion in vivo and in vitro (10, 11, 51, 52). However, the upstream pathways of Prox1 in LECs are still poorly understood, except for the Sox18 transcription factor and RAF1/ERK signaling (26, 53). In this study, we confirmed that Klf4 is upregulated in flow-exposed dermal BECs and LECs in vitro and in developing SC ECs in vivo (28, 54). Moreover, previous studies indicated that even if the current of aqueous humor is low, the presence of AHO itself is enough to actively modulate the behaviors of SC ECs, which is in agreement with our data (15). We demonstrated that Prox1 and Klf4 expressions in SC are simultaneously modulated in a temporal manner and are associated with AHO levels during developmental stage and adulthood. Accordingly, we addressed that the defective integrities of SC could be explained by the plasticity of Prox1, which was dependent on the level of AHO. However, our experimental

conditions could not turn on the Prox1 expression in BECs. The failure of Prox1 upregulation in BECs by the shear stress could be due to multiple reasons: postnatal dermal BECs may not properly represent the molecular and cellular features of the primitive BECs that differentiate to SC ECs; the magnitude or nature of the shear stress generated in vitro may significantly differ from that of in vivo AHO, or AHO alone, although necessary, may not be sufficient for Prox1 upregulation and lymphatic differentiation of the primitive BECs. Further studies are needed to address the molecular basis of AHO-induced Prox1 upregulation in SC.

We found that Foxc2 in SC emerged from at least P7 and was retained through adulthood. Foxc2 expression is triggered by oscillatory shear stress in LECs (24). Because of the absence of a valve between SC and AV, it is postulated that the oscillatory pulse wave of aqueous humor from AV to SC, induced by the ocular pulse, blinking, and eye movements of normal eyes (55), might be associated with Foxc2 expression in SC. However, the heterogeneous Foxc2 expression that is only partly visible in Prox1$^+$ SC is contrasted with the distinct expression of that in lymphatic valve (24), thereby supporting the hypothesis of intermediate lymphatic phenotype in SC.

The senescence of SC in aged mice is quite similar to that in aged humans (46). However, there are only few works in the literature depicting the integrity of SC ECs, except decreased densities of transendothelial pores in SC ECs, depending on AHO with aging (56). We reveal that the impairment of the integrity of SC ECs manifests increased numbers of mesenchymal cells, including fibroblasts and myofibroblasts, on the outer wall of SC in aged mice or those in pathological conditions. This phenomenon can be correlated with the higher accumulated plaque-like material (presumed to be elastic fibers produced from fibroblasts) around SC in aged humans (57). Furthermore, the transition of SC ECs to mesenchymal cells can be interpreted as a temporary action taken to avoid apoptosis against the sublethal cellular stress resulting from deficient AHO (7). VEGF-C/VEGFR3 signaling is closely related to the development of SC, where the disturbance of this signaling induces growth retardation of SC, accompanied by the same phenotype in limbal LVs. However, the rescued morphology and lymphatic identity of SC in VEGF-C heterozygous mice at a later postnatal period indicates that VEGF-C is not the main growth factor for the development of SC.

In summary, our evidence strongly points to AHO as the main element to maintain SC integrity and identity and above all presents Prox1 as an accurate biosensor for SC. Considering our data, which support the reliability of using Prox1 to reflect the functionality of SC, further research to detect Prox1 expression in the SC of humans will allow for the early detection and prevention of IOP-induced pathologies such as glaucoma.

Methods

Mice. Specific pathogen–free C57BL/6J mice, Tie2-GFP (FVB/N) mice, and R26$^{mTmG/+}$ mice were purchased from the Jackson Laboratory. Prox1-GFP mice (17), *Vegfc*$^{+/LacZ}$ mice (34), and Prox1-Cre^{ERT2} mice (58) were transferred and bred in our pathogen-free animal facilities. Prox1-GFP mice were backcrossed for 6 or more generations to C57BL/6J. Tamoxifen (Sigma-Aldrich) was dissolved in corn oil (Sigma-Aldrich), and the resulting tamoxifen solution (2 mg) was injected into the peritoneal cavity 3 times every 2 days for adult mice aged 8 weeks for Prox1$^+$ cell labeling. All animals were fed ad libitum with a standard normal diet (PMI Lab) with free access to water. For anesthesia, mice were i.p. injected with anesthetic solution (ketamine, 40 mg/kg; and xylazine, 5 mg/kg).

Preparations and treatments of reagents. To produce recombinant proteins (sVEGFR3-Fc and dimeric-Fc), stable CHO cell lines that secrete these recombinant proteins were used as previously described (59). Recombinant proteins in supernatant were purified by column chromatography with protein A–agarose gel (Oncogene) using acid elution. After purification, the recombinant proteins were quantified using the Bradford assay and confirmed by Coomassie blue staining after SDS-PAGE. sVEGFR3-Fc (25 mg/kg) was injected daily from P1 to P6, and Fc was injected in the same manner as control. Mice were treated with anti–integrin β_1 functional blocking antibody (BD Biosciences, 25 mg/kg) or isotype-matched control antibody (BD Biosciences, 25 mg/kg) daily from P1 to P6.

Histological analyses. For H&E staining, corneas were fixed overnight in 4% paraformaldehyde (PFA). After tissue processing using standard procedures, samples were embedded in paraffin and cut into 3-μm sections followed by H&E staining. For immunofluorescence studies of whole-mounted or cross-sectioned corneas, eyes were fixed with 1% PFA for 30 minutes at room temperature. The corneas were microsurgically harvested by removing the other portions of the eye. Tissues were washed with PBS for 5 minutes 3 times. For the cross-section, samples were additionally dehydrated in 20% sucrose solution overnight and embedded in tissue-freezing medium (Leica). Frozen blocks were cut into 10-μm sections. IHC in whole-mounted retinas was performed as previously described (60). The whole corneas or sectioned corneas or retinas were incubated with 1 or more of the following antibodies: anti-CD31 (hamster monoclonal, clone 2H8; Millipore); anti-PDGFRβ (rat monoclonal, clone APB5; eBioscience); FITC-, or Cy3-conjugated anti–α-SMA (mouse monoclonal, clone 1A4; Sigma-Aldrich); anti-Prox1 (rabbit polyclonal; ReliaTech); anti-Prox1 (goat polyclonal; R&D); anti-VEGFR3 (goat polyclonal; R&D); anti-endomucin (rat polyclonal; Santa Cruz Biotechnology Inc.); anti-Itga9 (goat polyclonal; R&D); anti-podoplanin (hamster polyclonal; AngioBio); anti–VE-cadherin (rat monoclonal, clone 11D4.1; BD Biosciences — Pharmingen); anti–LYVE-1 (rabbit polyclonal; AngioBio); anti-collagen type IV (rabbit polyclonal; Cosmo Bio); anti-Sox18 (rabbit polyclonal; Aviva System Biology); anti-Foxc2 (sheep polyclonal; R&D); anti–integrin β_1 (rat monoclonal, clone 9EG7; BD Biosciences); anti-CD31 (rat monoclonal, clone MEC 13.3; BD Biosciences); anti-VEGFR2 (rabbit monoclonal, TO14; a gift from Rolf A. Brekken, Hamon Center for Therapeutic Oncology Research, University of Texas Southwestern Medical Center, Dallas, Texas, USA); anti–phosphohistone H3 (PH3) (rabbit polyclonal; Millipore); anti–caspase-3 (rabbit polyclonal; R&D); anti-Klf4 (goat polyclonal; R&D); anti-eNOS (mouse monoclonal; BD Bioscience); anti-vWF (rabbit polyclonal; Chemicon); anti-vimentin (goat polyclonal; Chemicon); anti–FSP-1 (rabbit polyclonal; Abcam); anti-desmin (rabbit monoclonal, clone Y66; Millipore); anti–MMP-2 (rabbit polyclonal; Abcam); anti–MMP-9 (goat polyclonal; R&D); and anti-TER119 (rat monoclonal, clone TER-119; eBioscience). After several washes, the samples were incubated for 4 hours at room temperature with the following antibodies: FITC-, Cy3- or Cy5-conjugated anti-hamster IgG antibody (Jackson ImmunoResearch); FITC-, Cy3-, or Cy5-conjugated anti-rabbit antibody (Jackson ImmunoResearch); FITC-, or Cy5-conjugated anti-rat

antibody (Jackson ImmunoResearch); Cy3-conjugated anti-sheep IgG antibody (Jackson ImmunoResearch); Cy3-conjugated anti-goat IgG antibody (Jackson ImmunoResearch). Goat Fab fragment anti-mouse IgG (Jackson ImmunoResearch) was used to block endogenous mouse IgG to use mouse antibody on mouse tissues.

For whole-mounted corneas or retinas, the samples were cut radially and then mounted in fluorescent mounting medium (Vector or DAKO). To measure the ROS level, Cell ROX Orange (Molecular Probes) was used according to the manufacturer's instruction. Corneas were stained with 5 μM of Cell ROX Orange and FITC-conjugated lectin (Sigma-Aldrich) for 1 hour at 37°C. To examine β-gal activity, the corneas were incubated with a staining solution (2 mM magnesium chloride, 5 mM potassium ferricyanide, 5 mM potassium ferrocyanide and 1 mg/ml 4-chloro-5-bromo-3-indolyl-β-D-galactopyranoside [X-gal] in PBS) at 37°C for 12 hours. SA–β-gal activity was detected with the senescence detection kit (Cell Signaling Technology) using the manufacturer's method. All immunofluorescent images were acquired using a Zeiss LSM 510 confocal microscope equipped with argon and helium-neon lasers (Carl Zeiss). The images stained with H&E or β-gal activity were captured by microscope equipped with CCD camera (Carl Zeiss).

Morphometric analyses. Morphometric measurements of areas and protein expression in SC were made on the whole-mounted or cross-sectioned tissues using a photographic analysis in ImageJ software (http://rsb.info.nih.gov/ij). The relative area of a SC was calculated as a percentage of $CD31^+$ area divided by its control area. To determine the relative expression of Prox1 and Klf4, intensities were calculated in the nucleus region of $CD31^+$ SC. As for the quantification of the relative expression including Prox1-GFP, Tie2-GFP, VEGFR2, VEGFR3, vWF, eNOS, Itga9, MMP-2, and MMP-9, intensities were measured in the $CD31^+$ SC area. The group with the highest intensity was normalized to 100%, from which the relative intensities of other groups were calculated. The numbers of $PH3^+$ and caspase-3^+ ECs were counted from the $CD31^+$ SC area of random 0.0265 mm^2 area. The percentage of perfused beads was calculated as red $beads^+$/FITC-$CD31^+$ SC area divided by the $CD31^+$ SC area. The expression of SA–β-gal was calculated as a percentage of the SA–β-gal $LacZ^+$ area in random 0.21 mm^2 regions. The expression of ROS was analyzed as ROS^+CD31^+ SC area divided by the total $CD31^+$ SC area. The expression of α-SMA, FSP-1, vimentin, and desmin on the outer wall of SC was calculated as a percentage of the positive area of each marker divided by $CD31^+$ SC area. All measurements were performed in at least 5 different SC per cornea, excluding the portion of the bifurcation of LPCAs, unless indicated otherwise. Radial length of BVs and number of filopodia in the retina were counted as previously described (60).

Intravital imaging. A custom-built scanning laser confocal microscopy system was used for in vivo imaging. A custom-developed scanner formed of an aluminum-coated polygonal mirror (MC-5; Lincoln Laser) and a galvanometer (6220H; Cambridge Technology) generated and delivered raster-scanning patterns to the back aperture of the objective lens. Three photomultiplier tubes (PMT, R9110; Hamamatsu) were used as fluorescence detectors. Corneas were examined using a ×60 objective lens, which provided a field of view of 170 μm × 170 μm (LUMFLN, numerical aperture [NA] = 1.1; Olympus). Images were displayed and stored at an acquisition rate of 30 frames per second with 512 × 512 pixels per frame by a custom-written software based on the Matrox Imaging Library. Each image was generated by averaging the noise over 90 frames to improve contrast and signal-to-noise ratio. Multiple images obtained at different depths were merged to clearly show the whole structure of SC.

Functional assay for AHO. To determine the rate of AHO, 500 nl of sterilized PBS containing 1% red fluorescent microspheres (1 μm in diameter; FluoSpheres; Molecular Probes) was injected into the anterior chamber using Nanoliter 2000 Microinjector (World Precision Instruments) \fitted with glass capillary pipettes under anesthesia. One hour after the injection, corneas were harvested for histologic analyses.

IOP measurement. IOPs were recorded with a tonometer (TonoLab; Tiolat) according to a previous report (61). IOP measurements were taken immediately after the mice lost consciousness by placing the tip of the pressure sensor approximately 1/8 inch from the central cornea. The average IOP was obtained after 5 measurements.

Artificially induced AHO modulation models. A previous report using a simulation model of the glaucoma surgery showed that an ocular puncture makes most of the flow go through the orifice (62). To generate the experimental ocular puncture model, eyes were punctured using a 31-gauge syringe needle (for postnatal mice) or 25-gauge syringe needle (for adult mice) at the temporal side of sclera located at around 0.5 mm (for postnatal mice) or 1 mm (for adult mice) away from the sclerocorneal junction under anesthesia. To expose the eyes of postnatal mice prior to puncture, excision was performed using a surgical blade on both sides of the eyelids at the initial stage. Baseline IOPs were obtained before puncture. To prevent spontaneous closure through wound healing, punctured sites were recanalized by puncturing daily with the following schedules: from P3 to P5 for postnatal mice, P5 to P7 for postnatal mice, P6 for postnatal mice, from P5 to P14 for postnatal mice, from P14 to P21 for postnatal mice, and 7 days for adult mice. For control, the surface of the opposite eye was scratched using microscissors.

To reduce AHO pharmacologically, only 1 eye per mouse treated topically with Cosopt (Merck & Co., Inc.), an IOP-lowering drug for glaucoma patients (a combined agent of β-adrenergic receptor inhibitor and carbonic anhydrase inhibitor) that inhibits the aqueous humor production in the ciliary body (27), from P5 to P7. The contralateral eye was treated with PBS containing 0.0075% benzalkonium chloride to be used as a control buffer. Twice daily, 5 μl of each eyedrop was applied. IOP was obtained 1 hour after eyedrop application, and corneas were harvested at P7.

To generate experimental glaucoma models, 4 μl of 6 μm beads (Polybead Microspheres; Polysciences Inc.), followed by 2 μl of viscoelastic solution (10 mg/ml hyaluronate sodium; Viscoat; Advanced Medical Optics Inc.), was injected into the anterior chamber of eyes using Nanoliter 2000 Microinjector (World Precision Instruments) fitted with glass capillary pipettes under anesthesia (63). For controls, PBS was injected in the same manner. Baseline IOPs were obtained before bead injection. Posttreatment IOP recordings were taken daily. At day 7 after bead injections, the corneas were harvested for histologic analyses. All posttreatment IOP recordings were taken daily. For all procedures that have been mentioned thus far, 0.3% Ofloxacin eyedrops (Cravit) were given on both eyes once per day every day.

To increase AHO mechanistically, 0.5 μl of aqueous humor aspirated from donor littermate eye was injected into the anterior chamber of eyes at P6 using Nanoliter 2000 Microinjector while mice were under anesthesia. To expose the eyes of pups prior to injection, excision was performed on both sides of eyelids. For control, the cornea of

the opposite eye was gently punctured using a tungsten needle (diameter, 100 μm). IOP was obtained before injection, 1 hour, and 24 hours after injection, and corneas were harvested at P7.

Reagents, cells, and culture condition for in vitro studies. Human neonatal primary dermal BECs and LECs were isolated and cultured as previously described (64). Laminar flow was generated to 1~2 dyne/cm^2 for specified time periods using an orbital shaker as previously reported (65). Total RNA and whole-cell lysates were isolated from primary BECs that were exposed to shear stress for 12 hours. RNA was subjected to RNA-Seq analyses at the USC Epigenome Center (GEO GSE58114). Adenovirus-expressing Klf4 was a gift from Chunming Liu (University of Kentucky, Lexington, Kentucky, USA) (66). Primary LECs were infected with adenovirus encoding GFP or Klf4. After 48 hours, cell lysates were obtained for Western blot analyses. Goat anti-Klf4 antibody was purchased from R&D Systems, and rabbit anti-Prox1 antibody was custom generated in a commercial company.

Luciferase assay. The putative binding region of Klf4 found in the first intron of Prox1 (chr1:212,229,489 - 212,229,614) was PCR-amplified from the genomic DNA from HEK293 cells using 2 primers (ATTGCTAGCAACCCCATCCTTCCGATCTC; CCCAATTCCCATTAGCCCAGA). The PCR fragments were digested with NheI and XhoI and directionally cloned into the NheI/XhoI sites of pGL3-Promoter (Promega Corp.). The resulting vector was named pGL3-promoter/enhancer. HEK293 cells were cotransfected with a combination of pGL3-promoter or pGL3-promoter/enhancer with an empty control vector (pcDNA3) or pCS2-FLAG-KLF4. After 48 hours, the cells were harvested and luciferase activity was determined and normalized based on total protein amount used.

ChIP. Primary LECs were cultured under the static or laminar flow condition for 12 hours and immediately subjected to ChIP as previously described (64) using anti-Klf4 antibody or control IgG. Sequences for the primers used are as follows: primer set 1: GAGCCTCCCATTACTCAGACC; GAGGCTCCCGCTTAGAAACT; primer set 2: TTGTTCTTTTGAGCCCTGCCATGTGAGTTC; CCTCCACCTGCT GCCTAAAGT).

RNA extraction and real-time RT-PCR analysis. The SC portions of corneas were harvested from eyes through removal of conjunctiva and the center portion of cornea to exclude limbal LVs. Total RNA was extracted from the samples using TRIzol Reagent (Invitrogen) according to the manufacturer's instructions, and 2 μg of the RNA was reverse transcribed into cDNA using SuperScript II Reverse Transcriptase (Invitrogen). Quantitative RT-PCR was performed with the indicated primers (see below) using Bio-Rad CFX96 Real-Time PCR Detection System (Bio-Rad). The RT-PCR data were analyzed with Bio-Rad CFX Manager software (Bio-Rad). Primers for the quantitative real-time PCR are as follows: *Prox1*; forward 5′-CAGCGGACTCTCTAGCACAG-3′ and reverse 5′-GCCTGCCAAAAGGGGAAAGA-3′.

Statistics. Values are presented as mean ± SD. Statistical differences between means were determined by unpaired 2-tailed Student's *t* test or 1-way ANOVA followed by the Student-Newman-Keuls test. Statistical significance was set at $P < 0.05$.

Study approval. Animal care and experimental procedures were performed with the approval of the Animal Care Committee of KAIST (2012-MS07). Mice were handled in accordance with the ARVO Statement for the Use of Animals in Ophthalmic and Vision Research. Human primary dermal BECs and LECs were isolated from deidentified, otherwise discarded neonatal foreskins; this use was approved by the University of Southern California Institutional Review Board.

Acknowledgments

We are grateful to Soo-Il Chang, Sujin Seo, Eun Soon Lee, and Tae-Chang Yang for their technical assistance. This study was supported by grants from the National Research Foundation funded by the Ministry of Science, ICT, & Future Planning, Korea (NRF-2011-0019268, to G.Y. Koh), the Korea Healthcare Technology R&D Project, Ministry of Health & Welfare (A110076, to G.Y. Koh), and the National Heart, Lung and Blood Institute/NIH (HL121036, HD059762, to Y.K. Hong).

Address correspondence to: Gou Young Koh, Graduate School of Medical Science and Engineering, KAIST, 373-1, Guseong-dong, Daejeon, 305-701, Korea. Phone: 82.42.350.2638; E-mail: gykoh@kaist.ac.kr. Or to: Young Kwon Hong, Departments of Surgery and of Biochemistry & Molecular Biology, Keck School of Medicine, University of Southern California, 1450 Biggy St., Los Angeles, California 90033, USA. Phone: 323.442.7825; E-mail: young.hong@usc.edu.

1. Ramos RF, Hoying JB, Witte MH, Stamer WD. Schlemm's canal endothelia, lymphatic, or blood vasculature? *J Glaucoma*. 2007;16(4):391–405.
2. Gabelt BT, Kaufman PL. Changes in aqueous humor dynamics with age and glaucoma. *Prog Retin Eye Res*. 2005;24(5):612–637.
3. Lei Y, Overby DR, Boussommier-Calleja A, Stamer WD, Ethier CR. Outflow physiology of the mouse eye: pressure dependence and washout. *Invest Ophthalmol Vis Sci*. 2011;52(3):1865–1871.
4. Fan BJ, Wiggs JL. Glaucoma: genes, phenotypes, and new directions for therapy. *J Clin Invest*. 2010;120(9):3064–3072.
5. Alm A, Nilsson SF. Uveoscleral outflow — a review. *Exp Eye Res*. 2009;88(4):760–768.
6. Aihara M, Lindsey JD, Weinreb RN. Aqueous humor dynamics in mice. *Invest Ophthalmol Vis Sci*. 2003;44(12):5168–5173.
7. Tomarev SI. Eyeing a new route along an old pathway. *Nat Med*. 2001;7(3):294–295.
8. Tammela T, Alitalo K. Lymphangiogenesis: Molecular mechanisms and future promise. *Cell*. 2010;140(4):460–476.
9. Alitalo K. The lymphatic vasculature in disease. *Nat Med*. 2011;17(11):1371–1380.
10. Mishima K, et al. Prox1 induces lymphatic endothelial differentiation via integrin alpha9 and other signaling cascades. *Mol Biol Cell*. 2007;18(4):1421–1429.
11. Johnson NC, et al. Lymphatic endothelial cell identity is reversible and its maintenance requires Prox1 activity. *Genes Dev*. 2008;22(23):3282–3291.
12. Yang Y, Oliver G. Transcriptional control of lymphatic endothelial cell type specification. *Adv Anat Embryol Cell Biol*. 2014;214:5–22.
13. Johnstone MA. A new model describes an aqueous outflow pump and explores causes of pump failure in glaucoma. In: Grehn F, Stamper R, eds. *Glaucoma*. Vol. 2. Heidelberg, Germany: Springer Berlin Heidelberg New York; 2006:3–34.
14. Overby DR, Stamer WD, Johnson M. The changing paradigm of outflow resistance generation: towards synergistic models of the JCT and inner wall endothelium. *Exp Eye Res*. 2009;88(4):656–670.
15. Zhou EH, et al. Mechanical responsiveness of the endothelial cell of Schlemm's canal: scope, variability and its potential role in controlling aqueous humour outflow. *J R Soc Interface*. 2012;9(71):1144–1155.
16. Danussi C, et al. Emilin1 deficiency causes structural and functional defects of lymphatic vasculature. *Mol Cell Biol*. 2008;28(12):4026–4039.
17. Choi I, et al. Visualization of lymphatic vessels by Prox1-promoter directed GFP reporter in a bacterial artificial chromosome-based transgenic mouse. *Blood*. 2011;117(1):362–365.

18. Corada M, et al. Sox17 is indispensable for acquisition and maintenance of arterial identity. *Nat Commun*. 2013;4:2609.
19. Petrova TV, et al. Lymphatic endothelial reprogramming of vascular endothelial cells by the Prox-1 homeobox transcription factor. *EMBO J*. 2002;21(17):4593–4599.
20. Schacht V, et al. T1α/podoplanin deficiency disrupts normal lymphatic vasculature formation and causes lymphedema. *EMBO J*. 2003;22(14):3546–3556.
21. Jackson DG. The lymphatics revisited: new perspectives from the hyaluronan receptor LYVE-1. *Trends Cardiovasc Med*. 2003;13(1):1–7.
22. Baluk P, et al. Functionally specialized junctions between endothelial cells of lymphatic vessels. *J Exp Med*. 2007;204(10):2349–2362.
23. Hirakawa S, et al. Identification of vascular lineage-specific genes by transcriptional profiling of isolated blood vascular and lymphatic endothelial cells. *Am J Pathol*. 2003;162(2):575–586.
24. Sabine A, et al. Mechanotransduction, PROX1, and FOXC2 cooperate to control connexin37 and calcineurin during lymphatic-valve formation. *Dev Cell*. 2012;22(2):430–445.
25. Bazigou E, et al. Integrin-α9 is required for fibronectin matrix assembly during lymphatic valve morphogenesis. *Dev Cell*. 2009;17(2):175–186.
26. Francois M, et al. Sox18 induces development of the lymphatic vasculature in mice. *Nature*. 2008;456(7222):643–647.
27. Whitlock NA, et al. Decreased intraocular pressure in mice following either pharmacological or genetic inhibition of ROCK. *J Ocul Pharmacol Ther*. 2009;25(3):187–194.
28. McCormick SM, et al. DNA microarray reveals changes in gene expression of shear stressed human umbilical vein endothelial cells. *Proc Natl Acad Sci U S A*. 2001;98(16):8955–8960.
29. Chiambaretta F, et al. Cell and tissue specific expression of human Kruppel-like transcription factors in human ocular surface. *Molecular vision*. 2004;10(108):901–909.
30. Jiang J, et al. A core Klf circuitry regulates self-renewal of embryonic stem cells. *Nat Cell Biol*. 2008;10(3):353–360.
31. Soufi A, Donahue G, Zaret KS. Facilitators and impediments of the pluripotency reprogramming factors' initial engagement with the genome. *Cell*. 2012;151(5):994–1004.
32. Planas-Paz L, Strilic B, Goedecke A, Breier G, Fassler R, Lammert E. Mechanoinduction of lymph vessel expansion. *EMBO J*. 2012;31(4):788–804.
33. Carlson TR, Hu H, Braren R, Kim YH, Wang RA. Cell-autonomous requirement for β1 integrin in endothelial cell adhesion, migration and survival during angiogenesis in mice. *Development*. 2008;135(12):2193–2202.
34. Karkkainen MJ, et al. Vascular endothelial growth factor C is required for sprouting of the first lymphatic vessels from embryonic veins. *Nat Immunol*. 2004;5(1):74–80.
35. Zeisberg EM, et al. Endothelial-to-mesenchymal transition contributes to cardiac fibrosis. *Nat Med*. 2007;13(8):952–961.
36. Medici D, Shore EM, Lounev VY, Kaplan FS, Kalluri R, Olsen BR. Conversion of vascular endothelial cells into multipotent stem-like cells. *Nat Med*. 2010;16(12):1400–1406.
37. Maddaluno L, et al. EndMT contributes to the onset and progression of cerebral cavernous malformations. *Nature*. 2013;498(7455):492–496.
38. Cone FE, Steinhart MR, Oglesby EN, Kalesnykas G, Pease ME, Quigley Ha. The effects of anesthesia, mouse strain and age on intraocular pressure and an improved murine model of experimental glaucoma. *Exp Eye Res*. 2012;99:27–35.
39. Sacca SC, Izzotti A, Rossi P, Traverso C. Glaucomatous outflow pathway and oxidative stress. *Exp Eye Res*. 2007;84(3):389–399.
40. Zode GS, et al. Reduction of ER stress via a chemical chaperone prevents disease phenotypes in a mouse model of primary open angle glaucoma. *J Clin Invest*. 2011;121(9):3542–3553.
41. Lee S, et al. Prox1 physically and functionally interacts with COUP-TFII to specify lymphatic endothelial cell fate. *Blood*. 2009;113(8):1856–1859.
42. Fritz-Six KL, Dunworth WP, Li M, Caron KM. Adrenomedullin signaling is necessary for murine lymphatic vascular development. *J Clin Invest*. 2008;118(1):40–50.
43. Makinen T, Adams RH, Bailey J, et al. PDZ interaction site in ephrinB2 is required for the remodeling of lymphatic vasculature. *Genes Dev*. 2005;19(3):397–410.
44. Wick N, et al. Lymphatic precollectors contain a novel, specialized subpopulation of podoplanin low, CCL27-expressing lymphatic endothelial cells. *Am J Pathol*. 2008;173(4):1202–1209.
45. Hagerling R, et al. A novel multistep mechanism for initial lymphangiogenesis in mouse embryos based on ultramicroscopy. *EMBO J*. 2013;32(5):629–644.
46. Liton PB, Challa P, Stinnett S, Luna C, Epstein DL, Gonzalez P. Cellular senescence in the glaucomatous outflow pathway. *Exp Gerontol*. 2005;40(8–9):745–748.
47. Acott TS, Kelley MJ. Extracellular matrix in the trabecular meshwork. *Exp Eye Res*. 2008;86(4):543–561.
48. Traub O, Berk BC. Laminar shear stress: mechanisms by which endothelial cells transduce an atheroprotective force. *Arterioscler Thromb Vasc Biol*. 1998;18(5):677–685.
49. Kolotuev I, Hyenne V, Schwab Y, Rodriguez D, Labouesse M. A pathway for unicellular tube extension depending on the lymphatic vessel determinant Prox1 and on osmoregulation. *Nat Cell Biol*. 2013;15(2):157–168.
50. Chen CY, et al. Blood flow reprograms lymphatic vessels to blood vessels. *J Clin Invest*. 2012;122(6):2006–2017.
51. Harvey NL, et al. Lymphatic vascular defects promoted by Prox1 haploinsufficiency cause adult-onset obesity. *Nat Genet*. 2005;37(10):1072–1081.
52. Srinivasan RS, Oliver G. Prox1 dosage controls the number of lymphatic endothelial cell progenitors and the formation of the lymphovenous valves. *Genes Dev*. 2011;25(20):2187–2197.
53. Deng Y, Atri D, Eichmann A, Simons M. Endothelial ERK signaling controls lymphatic fate specification. *J Clin Invest*. 2013;123(3):1202–1215.
54. Yet SF, et al. Human EZF, a Kruppel-like zinc finger protein, is expressed in vascular endothelial cells and contains transcriptional activation and repression domains. *J Biol Chem*. 1998;273(2):1026–1031.
55. Johnstone M, Martin E, Jamil A. Pulsatile flow into the aqueous veins: manifestations in normal and glaucomatous eyes. *Exp Eye Res*. 2011;92(5):318–327.
56. Allingham RR, Dekater AW, Ethier CR, Anderson PJ, Hertzmark E, Epstein DL. The relationship between pore density and outflow facility in human eyes. *Invest Ophth Vis Sci*. 1992;33(5):1661–1669.
57. Lütjen-Drecoll E, Shimizu T, Rohrbach M, Rohen J. Quantitative analysis of 'plaque material' in the inner-and outer wall of Schlemm's canal in normal-and glaucomatous eyes. *Exp Eye Res*. 1986;42(5):443–455.
58. Bazigou E, et al. Genes regulating lymphangiogenesis control venous valve formation and maintenance in mice. *J Clin Invest*. 2011;121(8):2984–2992.
59. Koh YJ, et al. Double antiangiogenic protein, DAAP, targeting VEGF-A and angiopoietins in tumor angiogenesis, metastasis, and vascular leakage. *Cancer Cell*. 2010;18(2):171–184.
60. Lee J, et al. Angiopoietin-1 guides directional angiogenesis through integrin alphavbeta5 signaling for recovery of ischemic retinopathy. *Sci Transl Med*. 2013;5(203):203ra127.
61. Reitsamer HA, Kiel JW, Harrison JM, Ransom NL, McKinnon SJ. Tonopen measurement of intraocular pressure in mice. *Exp Eye Res*. 2004;78(4):799–804.
62. Villamarin A, Roy S, Hasballa R, Vardoulis O, Reymond P, Stergiopulos N. 3D simulation of the aqueous flow in the human eye. *Med Eng Phys*. 2012;34(10):1462–1470.
63. Pease ME, Cone FE, Gelman S, Son JL, Quigley HA. Calibration of the TonoLab tonometer in mice with spontaneous or experimental glaucoma. *Invest Ophthalmol Vis Sci*. 2011;52(2):858–864.
64. Choi I, et al. 9-cis retinoic acid promotes lymphangiogenesis and enhances lymphatic vessel regeneration: therapeutic implications of 9-cis retinoic acid for secondary lymphedema. *Circulation*. 2012;125(7):872–882.
65. dela Paz NG, Walshe TE, Leach LL, Saint-Geniez M, D'Amore PA. Role of shear-stress-induced VEGF expression in endothelial cell survival. *J Cell Sci*. 2012;125(pt 4):831–843.
66. Evans PM, Chen X, Zhang W, Liu C. KLF4 interacts with β-catenin/TCF4 and blocks p300/CBP recruitment by β-catenin. *Mol Cell Biol*. 2010;30(2):372–381.